Available online at www.sciencedirect.com
ScienceDirect
Planetary and Space Science 56 (2008) 917–926
Planetary and Space Science
www.elsevier.com/locate/pss

Correction of the ionospheric distortion on the MARSIS surface sounding echoes

J. Mouginot[a,*], W. Kofman[a], A. Safaeinili[b], A. Herique[a]

[a]Laboratoire de Planétologie de Grenoble, CNRS/UJF, 38041 Grenoble Cedex, France
[b]Jet Propulsion Laboratory, California Institute of Technology, Pasadena, CA 91109, USA

Received 27 June 2007; received in revised form 14 January 2008; accepted 15 January 2008
Available online 6 February 2008

Abstract

Mars Advanced Radar for Subsurface and Ionospheric Sounding (MARSIS) on the Mars Express (MEX) spacecraft has made numerous measurements of the Martian surface and subsurface. However, all of these measurements are distorted by the ionosphere and must be compensated before any analysis. We have developed a technique to compensate for the ionospheric distortions. This technique provides a powerful tool to derive the total electron content (TEC) and other higher-order terms of the limited expansion of the plasma dispersion function that are related to overall shape of the electron column profile. The derived parameters are fitted by using a Chapman model to derive ionospheric parameters like n_0, electron density primary peak (maximum for solar zenith angle (SZA) equal 0), and the neutral height scale H.

Our estimated ionospheric parameters are in good agreement with Mars Global Surveyor (MGS) radio-occultation data. However, since MARSIS does not have the observation geometry limitations of the radio occultation measurements, our derived parameters extend over a large range of SZA for each MEX orbit.

The first results from our technique have been discussed by Safaeinili et al. [2007, Estimation of the total electron content of the Martian ionosphere using radar sounder surface echoes. Geophys. Res. Lett. 34, L23204, doi:10.1029/2007GL032154].

Keywords: Mars; Ionosphere; MARSIS; Ionospheric dispersion compensation; Total electron content

1. Introduction

The radar signals sent by Mars Advanced Radar for Subsurface and Ionospheric Sounding (MARSIS) on board Mars Express (MEX) pass through the Martian ionosphere. Therefore the MARSIS pulses are distorted due to the fact that their frequencies are close to the ionospheric plasma frequency, which can range from about 3.9 MHz during day to less than 1 MHz on the night side (Gurnett et al., 2005).

The radar pulse from MARSIS has a bandwidth of 1 MHz, and as a result it is broadened significantly in addition to being delayed. This broadening of the pulse causes the smearing of the radargram. Correction for ionospheric effects must be made to re-sharpen the pulse.

This ionospheric dispersion is a well-known effect due to the fact that the refractive index of ionosphere, or equivalently, the velocity of the radio wave in the ionosphere, depends on the radio wave frequency (Budden, 1985). Specifically, the impact of the Martian ionosphere on the radio wave have been detailed in the article by Safaeinili et al. (2003) where methods to correct the signal have been proposed. The method described in this paper is based on the method proposed by Safaeinili et al. (2003), however, we significantly improve the estimation performance by introducing an additional constraint, which is to match the surface echoes position at real surface altitude. Our method corrects the signal by matching the surface echo to the filter (surface altitude), while also taking the ionosphere into the account. The correction of phase of signals is done using the limited series expansion of the refractive index of plasma. This correction permits a good detection of surface and subsurface echoes. The beneficial

*Corresponding author. Tel.: +33 4 76 51 41 53.
E-mail address: jeremie.mouginot@obs.ujf-grenoble.fr (J. Mouginot).

0032-0633/$ - see front matter © 2008 Elsevier Ltd. All rights reserved.
doi:10.1016/j.pss.2008.01.010

by-product from the correction of ionosphere effect is the total electron count (TEC) of the ionosphere.

2. MARSIS instrument

MARSIS on board MEX can work in two different modes.

Here we report only the mode known as the subsurface sounding mode (Picardi et al., 2005). The subsurface sounding uses 4 different frequency bands that are centered to 1.8, 3, 4, and 5 MHz, respectively, generally called band 1, 2, 3, and 4. Each band is 1 MHz wide. In this article, we will refer to the central frequency of each band but we must keep in mind that these bands are large.

MARSIS emits and receives 127 pulses in each of the two operation bands for a total of 254 pulses/s. The choice of two operation bands depends of course on the solar zenith angle (SZA) and so on the plasma frequency. These pulses are integrated over 1 s to increase the signal-to-noise ratio (SNR) and reduce the volume of data. The MARSIS always operates two soundings with two different bands simultaneously, which allow us to study the response of the surface and subsurface, as the function of the frequency. The second mode or active ionospheric sounding (AIS) mode studies the ionosphere with a quasi-wave tone from about 0.1 to 5.5 MHz (Gurnett et al., 2005).

MARSIS can operate its subsurface mode when the spacecraft altitude is lower than 900 km. The MEX spends approximately 30 min per orbit under 900 km. The lower altitude is about 270 km at the periapse. The latitude and longitude of MEX orbit changes for each orbit and optimal MARSIS orbit sounds a half-hemisphere, which allows a survey of the entire Martian surface.

3. Ionospheric signal distortion

The ionosphere induces a frequency-dependent phase shift that results in the defocusing of the radargram (Fig. 1). This phenomenon is well known and described by Budden (1964) and Safaeinili et al. (2003). The phase shift term $\Delta\varphi$ is described by the equation

$$\Delta\varphi(\omega) = \frac{2\omega}{c}\int_{h_1}^{h_2} \Re(n-1)\,\mathrm{d}h, \tag{1}$$

$$n = \sqrt{1-\frac{\omega_p^2}{\omega^2}} \cong 1 - \frac{1}{2}\left(\frac{\omega_p^2}{\omega^2}\right) - \frac{1}{8}\left(\frac{\omega_p^2}{\omega^2}\right)^2 - \frac{1}{16}\left(\frac{\omega_p^2}{\omega^2}\right)^3, \tag{2}$$

where n is the refractive index, $\omega = 2\pi f$ is the pulsation of the radio wave signal, ω_p the plasma pulsation, c the speed of light in a vacuum, h_1 and h_2 the lower and upper altitude traversed in the ionosphere.

The plasma frequency, f_p (Hz) is given by

$$f_p = \frac{q_e}{2\pi\sqrt{\varepsilon_0 m_e}}\sqrt{n_e} \approx 8.98\sqrt{n_e}, \tag{3}$$

where n_e is the electron density (m^{-3}), $q_e = 1.6\times10^{-9}$ is the electron charge (Coulomb), $m_e = 9.11\times10^{-31}$ is the electron mass (kg), $\varepsilon_0 = 8.854\times10^{-12}$ is the free-space permittivity (F/m).

Using Eqs. (2) and (3), Eq. (1) can be rewritten as

$$\Delta\varphi(f) = \frac{4\pi}{c}\left[\frac{40.32}{f}\int_{h_1}^{h_2} n_e\,\mathrm{d}h + \frac{812.851}{f^3}\int_{h_1}^{h_2} n_e^2\,\mathrm{d}h + \frac{32774.2}{f^5}\int_{h_1}^{h_2} n_e^3\,\mathrm{d}h\right]. \tag{4}$$

In the following, we use the denotation α_1, α_2, α_3 and a_1, a_2, a_3 to describe the different order terms of Eq. (4). These terms are defined by

$$\alpha_i = \int n_e^i(h)\,\mathrm{d}h, \tag{5}$$

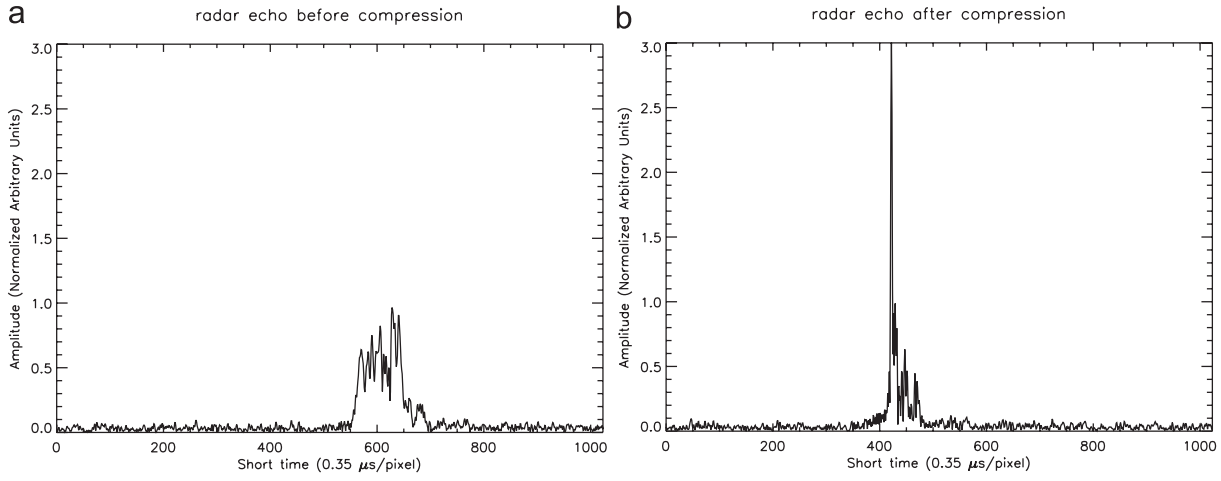

Fig. 1. (a) MARSIS pulse after ionospheric two-way propagation represented in time domain. One can see a spread delayed pulse compared with the same pulse (b) after ionospheric correction (pulse number 389 of the 2450th Mars Express orbit).

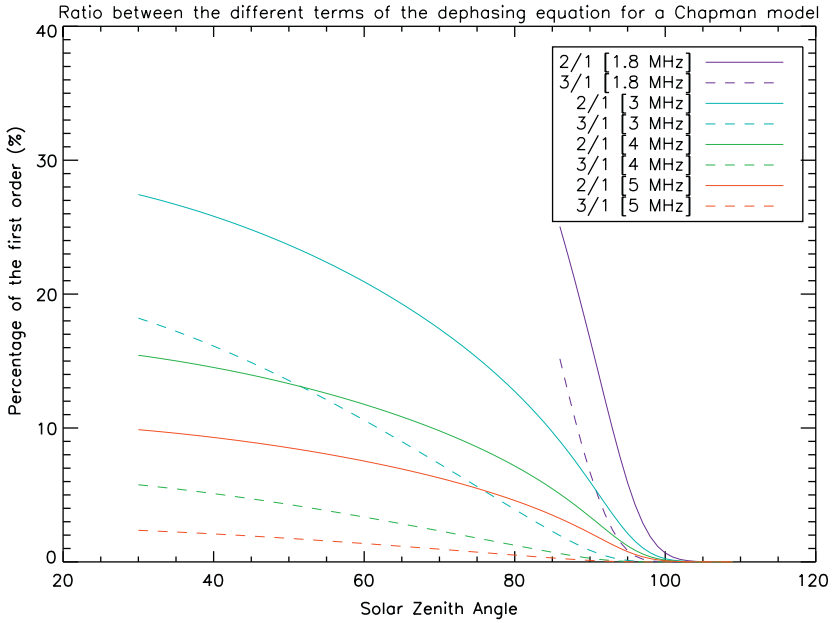

Fig. 2. Ratio in percentage between the expansion terms of phase shift Eqs. (4) and (5) as a function of the solar zenith angle. The different term are calculated with a Chapman model using typical values for Martian ionosphere. Solid lines correspond to the ratio between the second and the first term and dashed lines to the ratio of third and first term. Different colors are taken for each frequency (red: 5 MHz, green: 4 MHz, light blue: 3 MHz, blue: 1.8 MHz).

$$a_1 = 40.32 \times \alpha_1 \times \frac{4\pi}{c},$$

$$a_2 = 812.851 \times \alpha_2 \times \frac{4\pi}{c},$$

and

$$a_3 = 32774.2 \times \alpha_3 \times \frac{4\pi}{c}. \quad (6)$$

Finally, the phase shift in Eq. (4) can be rewritten as

$$\Delta\varphi(f) = \frac{a_1}{f} + \frac{a_2}{f^3} + \frac{a_3}{f^5}. \quad (7)$$

It should be noted that our measurements give the TECs between the spacecraft and the ground. The altitude of the main electronic density peak is around 130–150 km (Bougher et al., 2001, 2004; Fox and Yeager, 2006). We can consider that h_1 and h_2 in Eq. (4) are, respectively, equal to 0 and infinity, the contribution of higher altitudes to the TEC is small.

Other significant impacts of the Martian ionosphere on the radar signal are attenuation and the Faraday rotation (Safaeinili et al., 2003). MARSIS subsurface sounding mode operates primarily for SZA higher than 60°. Furthermore, in the case of SZA less than 90° the radar is operated with the band frequency at 3 MHz and above. So to first order, the attenuation due to the electron-neutral collisions in the ionosphere (Safaeinili et al., 2003; Nielsen et al., 2007) and the Faraday rotation can be considered negligible.

Fig. 1 shows an ionospheric distortion of the radar pulse. The signal after a two-way propagation in the ionosphere is delayed and spread. Eq (4) shows the dependence of phase shift for the first three terms of the expansion of the refractive index n, these terms are called a_1, a_2, a_3 (Eq. (6)). The first term a_1 depends on the integral of electron density or TEC. In most cases, under high SZA conditions (i.e. during the night), the higher-order terms have less influence on the total phase distortion.

The higher-order terms (Eq. (4)) are not negligible for lower SZA. In Fig. 2, we plot the ratio between $a_2/(a_1 f^2)$ and $a_3/(a_1 f^4)$ for typical parameters of Martian ionosphere. The terms a_1, a_2 and a_3 in Fig. 2 are computed using a Chapman model for the electron density profile (Chapman, 1931). The typical parameters for a Chapman model on Mars would be neutral height scale equal to 10 km and n_0 equal $2 \times 10^{11}\,\mathrm{m}^{-3}$ (Fox and Yeager, 2006). One can see in Fig. 2 that the second and the third term can be, respectively, more than 15% and 5% of the first term even using the upper band 4 and 5 MHz for low SZA. However, since during operation the lowest bands are used only during the night, the contribution of higher-order terms is never higher than 10% and 20% of the first order for the band 1.8 MHz. This study identifies situations where it is necessary to use three or more terms in Eq. (2).

4. Technique for correction of ionospheric distortion

4.1. Technique

MARSIS radar uses a linearly modulated chirp $s(f)$. The signal after traversing the ionosphere can be written as $s_1(f) = s(f)\exp(-j\varphi(f))$ where the phase terms include the propagation through the free space

$$\varphi_{\mathrm{space}} = \frac{2\omega}{c}\int \mathrm{d}h. \quad (8)$$

The phase perturbation $\Delta\varphi$ is indicated in Eq. (1). Ideally, the received signal is correlated with a reference ideal chirp (matched filter) to produce a narrow and well-defined radar pulse. This technique maximizes SNR at the receiver. The phase disturbance results in a poor compression of the chirp that causes a broadening of the compressed radar pulse. To improve the output signal we use the strategy for correcting the signal proposed by Safaeinili et al. (2003). This strategy consists of the modification of the phase of the arriving signal, by introducing the phase correction developed in Eqs. (1)–(7)

$$S_{\text{compressed}}(f) = C^{*}_{\text{chirp}}(f) S_1(f) \exp(\mathrm{j}\Delta\varphi(f)), \tag{9}$$

where f is covering 1 MHz bandwidth.

The spectrum of the distorted signal $s_1(f)$ is multiplied by the exponential of this corrective term and than compressed by multiplying by the conjugate copy of the chirp signal (Eq (9)). As we do not know a priori what the coefficients are that we should use to correct the signal we are using an optimization method to select them. We explore the set of the parameters (integrals of the n_e, n_e^2 and n_e^3) in such a way, as to obtain the maximization of the amplitude of the signal reflected by the surface at the output of matched filter. This maximization of the signal ensures that the signal is well compressed. To implement this procedure and to make this procedure efficient we have to introduce some physical constraints that we discuss in the next sections. Our correction is divided into two steps as described in next sections. First step uses a Gaussian model as electron density profile and allow us to determine initial conditions for the parameters a_1, a_2 and a_3 (Eq. (6)) used in the second correction step. When the optimal compression is obtained as a by-product we derive the TEC.

5. MOLA altitude constraint

The first constraint is given by the altitude of the spacecraft and the propagation time corresponding to this altitude. The phase of the surface reflected signal measured by the receiver is

$$\varphi_{\text{measured}} = \varphi_{\text{space}} + \Delta\varphi. \tag{10}$$

In the maximization procedure $\varphi_{\text{estimated}} = \varphi_{\text{measured}} - \Delta\varphi_{\text{correction}}$ is the estimated phase corresponding to the height of the spacecraft.

To estimate the $\Delta\varphi_{\text{correction}}$ we are imposing that $\varphi_{\text{estimated}}$ should be close to the φ_{space} given by the distance of the MEX to the surface as estimated from the Mars Orbiter Laser Altimeter (MOLA) data (Smith et al., 2003) within a ± 0.6 km limit and the output of matched filter should be maximum. In practice we use the time delay instead of the phase.

6. Electron profile shape constraint

In order to start the optimization procedure one should provide the initial conditions. For this we use the simplified electron density profile that is a Gaussian one

$$n_e(z) = n_0 \exp\left[-\frac{(h-h_0)^2 \sec\chi}{2H^2}\right], \tag{11}$$

where n_0 is the maximum of the electron density, H is the scale height and χ is the SZA.

With this profile we calculate the phase correction that depends on two unknown parameters TEC and the scale height H. Using a Gaussian approximation of electron density with altitude, the solution of the integrals of n_e, n_e^2 and n_e^3 (see Eq. (4)) are easily derived by

$$\int n_e^i(h) = \frac{1}{\sqrt{i}}\left(\frac{\sec\chi}{2\pi}\right)^{(i-1)/2} \frac{\mathrm{TEC}^i}{H^{i-1}}. \tag{12}$$

Eq. (13) shows this dependence. The phase correction depends also on the SZA that is known parameter

$$\Delta\varphi(f) = \frac{2}{c}\left[\frac{253.34}{f}\mathrm{TEC} + \frac{1440.76\sqrt{\sec\chi}}{f^3}\frac{\mathrm{TEC}^2}{H} + \frac{18922.4\sec\chi}{f^5}\frac{\mathrm{TEC}^3}{H^2}\right] \tag{13}$$

This simplified formula allows integration for only two parameters with minor impact on the quality of the estimation. In practice, the value of H varies between 8 and 30 km, which is the expected range for the height scale of the Mars atmosphere (Krymskii, 2004; Gurnett et al., 2005; Nielsen et al., 2007). The introduction of the simplified model of the ionosphere in general will result in suboptimal estimation of the phase. However, this simplified model will provide good initial conditions for the second step of the correction.

7. Optimization method

In order to obtain the best solution for the signal compression one has to explore the set of parameters for the phase correction terms in an independent way. So in this approach, we are searching to optimize the SNR of the surface echo. For the third-order correction one has three free parameters, a_1, a_2 and a_3 as defined previously (Eq. (7)), to explore.

If the first correction step is close to the optimal solution (the best SNR), then we only need to explore a_1, a_2 and a_3 around the values found previously. So the previous correction values provide the starting point $[a_{10}, a_{20}, a_{30}]$. At the start, we build a space covering the $\pm 20\%$ of the first parameters a_{10} and $\pm 50\%$ of the following ones (a_{20} and a_{30}). This is done to minimize the search time relying on the fact that usually we do have a good first-order estimate for the parameters. Effectively, we must compute a fast fourier transform (FFT) for each a_1, a_2 and a_3 combination (correction in frequency domain and checking in time domain). For each orbit, we process signals measured for two transmitted bands together.

Another important point is that the optimum solution should be the same for the different bands because a_1, a_2 and a_3 depend only on the electron profile of the ionosphere and not on the frequency. So we optimize the SNR of each frequency band. Once the optimum is found the next iteration center the new cube on the new solution then the step is decreased and the new iteration starts. The process is stopped when the increase in the maximum of the compressed signal achieves the optimum within a given percentage of the previous value (respectively, 20%, 40%, and 40% for a_1, a_2 and a_3). Figs. 1a and b show only one frame before and after our ionospheric compensation, and in Fig. 3 we show all frames for one orbit (called radargram). It can be seen from the narrow width of the echoes that the compression works well. The surface echoes are strong and the subsurface echoes are very well compressed. The fact the subsurface echoes are very narrow indicates that the losses inside the subsurface are

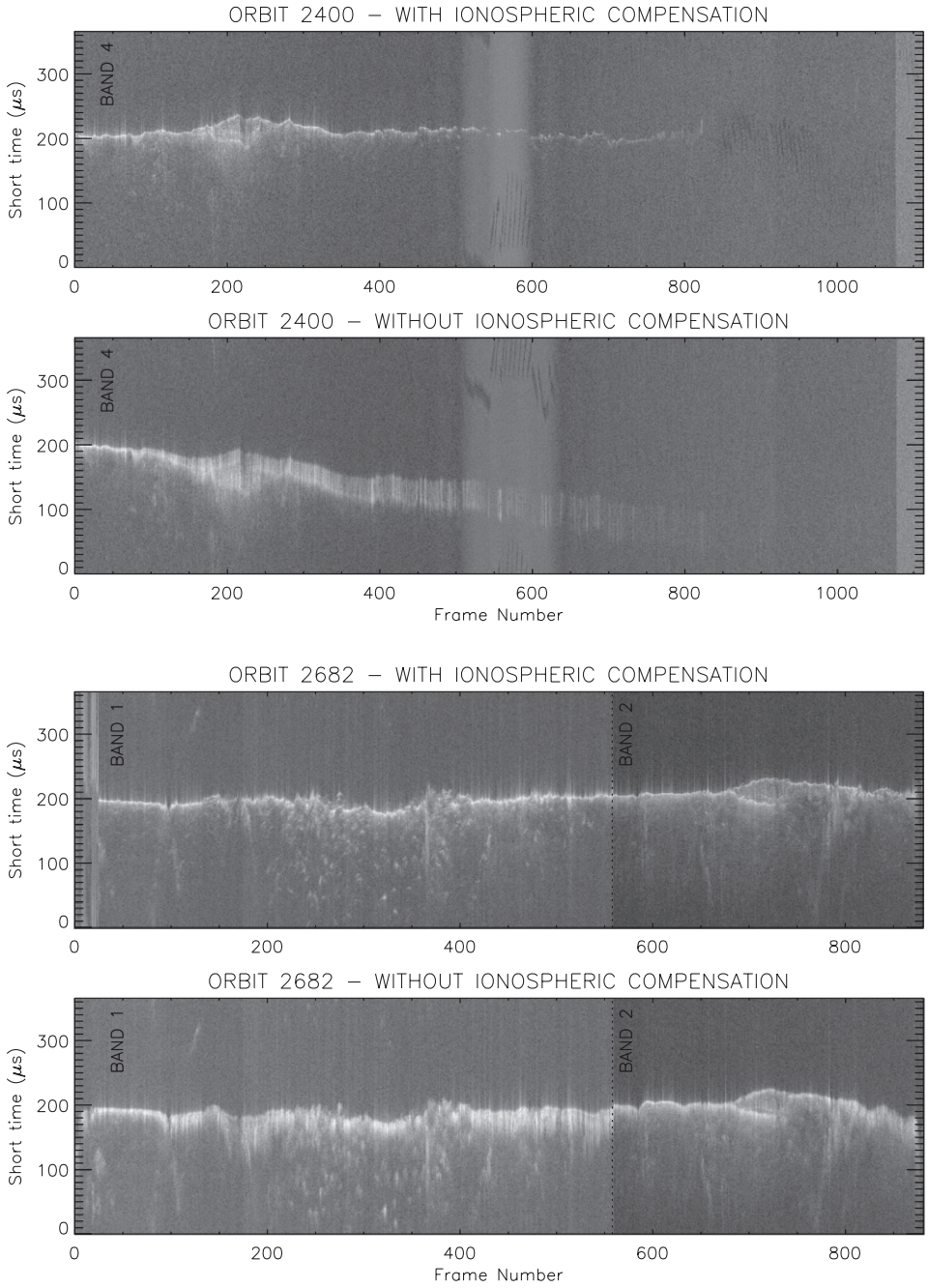

Fig. 3. Radargrams of the orbit 2400 and 2682. These observations were done on the Southern Hemisphere, respectively, at November 25, 2005 and February 12, 2006. The vertical axis is the short time that corresponds to the depth of penetrating signal. The horizontal axis corresponds to successive measurements. The white first line is the surface echo followed by the subsurface signal. Radargrams are presented two by two (first: signal after correction, second signal before correction), each couple is, respectively, called (a) and (b). (a) Shows the correction for the upper band (5 MHz) and (b) for the lower bands (1.8 and 3 MHz). Almost all MARSIS frequency bands are represented here.

almost independent of frequency otherwise, it would cause the spreading since the signal has a fractional bandwidth larger than 20%. Fig. 3 shows the radargrams for two bands. In Fig. 3a, we show the band at 5 MHz (band 4) before compression and after the correction of the phase. Fig. 3b shows similar plots with the lower bands at 1.8 MHz (band 1) and 3 MHz (band 2), respectively. One can see the effectiveness of our procedure and that even the lowest frequencies are well corrected. This procedure is used routinely to correct for ionospheric distortions.

8. Application to MARSIS data

We apply this technique to the MARSIS data in order to obtain well-compressed radargrams. As a beneficial by-product of the surface echo correction for ionospheric effects we derive the TEC for every 2 s. The TEC value is directly linked with the a_1 or α_1 parameter. In Fig. 4 we show the derived values of TEC for ones of the orbits. This figure shows the typical values of the TEC as functions of the SZA. Usually for SZA smaller than 50–55° the signal is lost, this is due to the strong absorption and distortion of the signal by the ionosphere.

To study the behavior of the ionosphere using whole set of data, we have used a Chapman model as the electron density profile to model α_1, α_2, and α_3. Then we fitted measured parameters.

This Chapman model (Chapman, 1931) (see formula (13)) of the ionospheric electron density profile is generally defined as

$$n_e(z,\chi) = n_0 \exp(-0.5(1 - z - Ch(d,\chi)\exp(-z))), \quad (14)$$

where $z = h - h_0/H, d = R + h/H$, χ the solar zenith angle, $R = 3396 \times 10^3$ m the radius of Mars (m), h the altitude (m), h_0 the altitude of maximum of production of ionization (m) and Ch the Chapman incidence function (Chapman, 1931) defined by

$$Ch(d,\chi) = d\sin\chi \int_0^x \exp\left(d - d\frac{\sin\chi}{\sin\alpha}\right)\mathrm{cosec}^2(\alpha)\,\mathrm{d}\alpha.$$

In this approach, we assume that during an orbit n_0 and H are constant parameters of the ionosphere and we estimate these parameters in taking advantage of the three terms of the ionosphere phase compensation (Eqs. (4) and (5)). Using the Chapman model, we have computed, for several conditions of n_0 and H, the terms α_1, α_2 and α_3 (Eq. (5)) as functions of χ as defined by

$$\alpha_1 = n_0 H \int \exp(-0.5(1 - z - Ch(H,\chi)\exp(-z)))\,\mathrm{d}z,$$

$$\alpha_2 = n_0^2 H \int \exp(-(1 - z - Ch(H,\chi)\exp(-z)))\,\mathrm{d}z, \quad (15)$$

$$\alpha_3 = n_0^3 H \int \exp(-1.5(1 - z - Ch(H,\chi)\exp(-z)))\,\mathrm{d}z.$$

Fig. 5 shows the behavior of the TEC(χ) as a function of χ for varying H. In Fig. 5, n_0 was fixed at 2×10^{11} m^{-3} and H varies from 5 to 30 km. The H range was chosen arbitrarily and covers a more large range than expected values for Martian ionosphere. The parameter n_0 is a factor whereas H appears also in Chapman incidence function Ch nevertheless the effect of n_0 and H on TEC looks very similar. The main difference comes from the behavior of TEC during sunrise or sunset at SZA near 90°. An increase

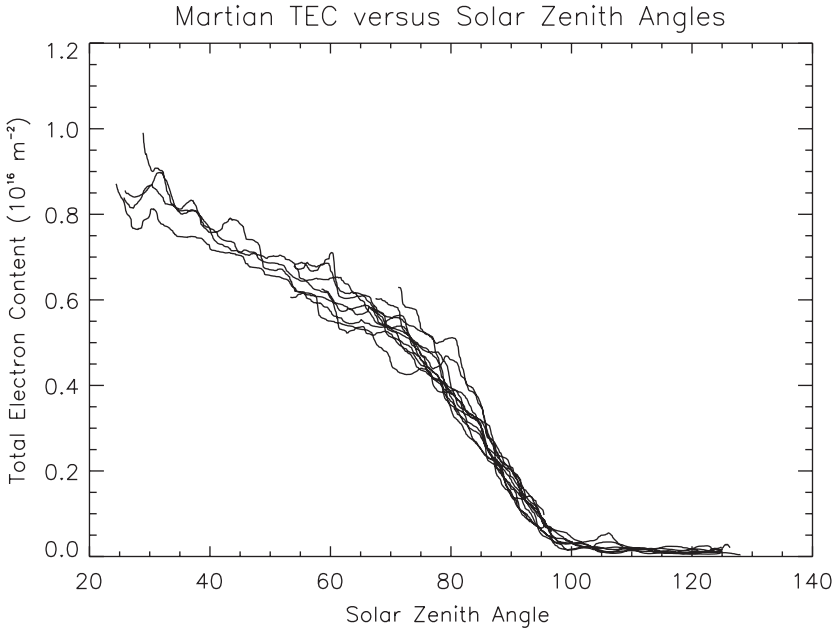

Fig. 4. Total electron content as a function of the solar zenith angle as measured by MARSIS surface sounding mode (MEX orbit 2392, 2393, 2398, 2414, 2540, 2541, 2543, 2544, 2545, 2575, 2604). Each continuous line represents an orbit. The total electron content is provided by a_1 term in the ionospheric correction. Here we show a range of SZA between 20° and 130° but mostly the signal is lost below 50–60°.

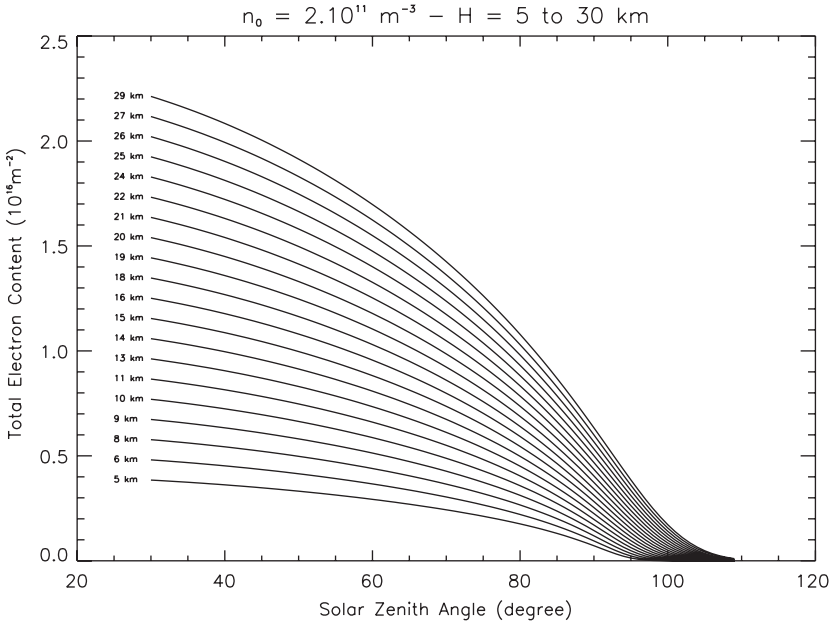

Fig. 5. Total electron content as a function of solar zenith angle in a Chapman model with H (neutral height scale) varying by 5–30 km.

of H shifts the TEC "rise" increases to larger SZAs whereas n_0 is just an amplitude factor. H variation has a bigger impact for SZA between 80° and 100°, so we need to use this range to fit the data and separate the parameters H and n_0.

The TEC above 100° does not improve the fit of data because TEC values are very low and flat (night side). And most of the time, the signal is lost for SZA below 55°, so our TEC estimation is very bad. Therefore, we take into account only the orbits, which cover the SZA range from 60° to 100°.

To compare α_1, α_2, α_3 estimated by the ionospheric correction, we must normalize α_1, α_2, α_3 because they can vary by many orders of magnitude. This is due to the fact that each of these terms depends on $\int n_e(h)\,dh$, $\int n_e^2(h)\,dh$, $\int n_e^3(h)\,dh$.

The minimization procedure minimizes

$$\varepsilon^2(n_0,H)=\sum_{\mathrm{SZA}}\frac{\varepsilon_1^2}{\alpha_1^2(\chi_{70})}+\frac{\varepsilon_2^2}{\alpha_2^2(\chi_{70})}+\frac{\varepsilon_3^2}{\alpha_3^2(\chi_{70})}, \tag{16}$$

where $\varepsilon_i^2(n_0,H)=\left(\alpha_i-\int n_e^i(z)\,dz\right)^2$ and χ_{70} is the SZA at 70°.

This normalization can be explained as the minimization of the weighed sum, when the weights are proportional to the errors that in turn are proportional to the measured values. As described previously in this section, the integrals $\int n_e^i(h)\,dh$ were calculated using Chapman model for the electron density profile.

In this case where we use minimization of α_1, α_2, α_3 at the same time, n_0 and H are more decoupled than in the case of a fit with only α_1 (see Eqs. (4), (5) and (12)). Fig. 6 represents the fit using α_1, α_2, and α_3 for the orbit 2454. We also plot in dot-dashed lines the fit for $\min(\varepsilon)+\Delta\varepsilon$ ($\Delta\varepsilon=50\%\min(\varepsilon)$). One can see the good agreement between the fit and the data; therefore we can say that a simple Chapman layer is good enough description of the Martian ionosphere below 200 km. We obtain typical values of n_0 and H as 9.5×10^3 m and $2\times10^{11}\,\mathrm{m}^{-3}$ (Safaeinili et al., 2007). The deviation on n_0 and H, which corresponds to dot-dashed lines in Fig. 6 is about $0.3\times10^{11}\,\mathrm{m}^{-3}$ and 1.2×10^3 m.

This also shows that the Mars ionosphere below 200 km behaves as the terrestrial E region where the production of ionization is equalized by losses by recombination, the losses depending in this ionospheric region on n_e^2 (Banks and Kockarts, 1973).

9. TEC determination sensitivity

It is important, for future applications to estimate how accurate is the TEC derivation. As defined in the previous sections, our correction method chooses the best SNR as criteria to compress the signal. To study the sensitivity, we evaluate the variation of correction within some acceptable deviation from the best SNR. The difference in SNR between raw and corrected data is 16–19 dB (19 dB for the pulse of Fig. 1). Therefore, we evaluate the range variability of ionospheric parameters for which the signal power loss is less than 1 dB compared with the best correction. One decibel is the arbitrary choice justified by the fact that we believe that our correction is efficient within 1 dB sensitivity. For instance, to measure the a_1 variability, we increase or decrease it until SNR equals best SNR minus 1 dB.

This variability depends of course on the frequency bands used in the given observation. As the correction is inversely proportional to frequency (see Eq. (7)), for lower band a small change in a_1, a_2, a_3 terms implies a larger

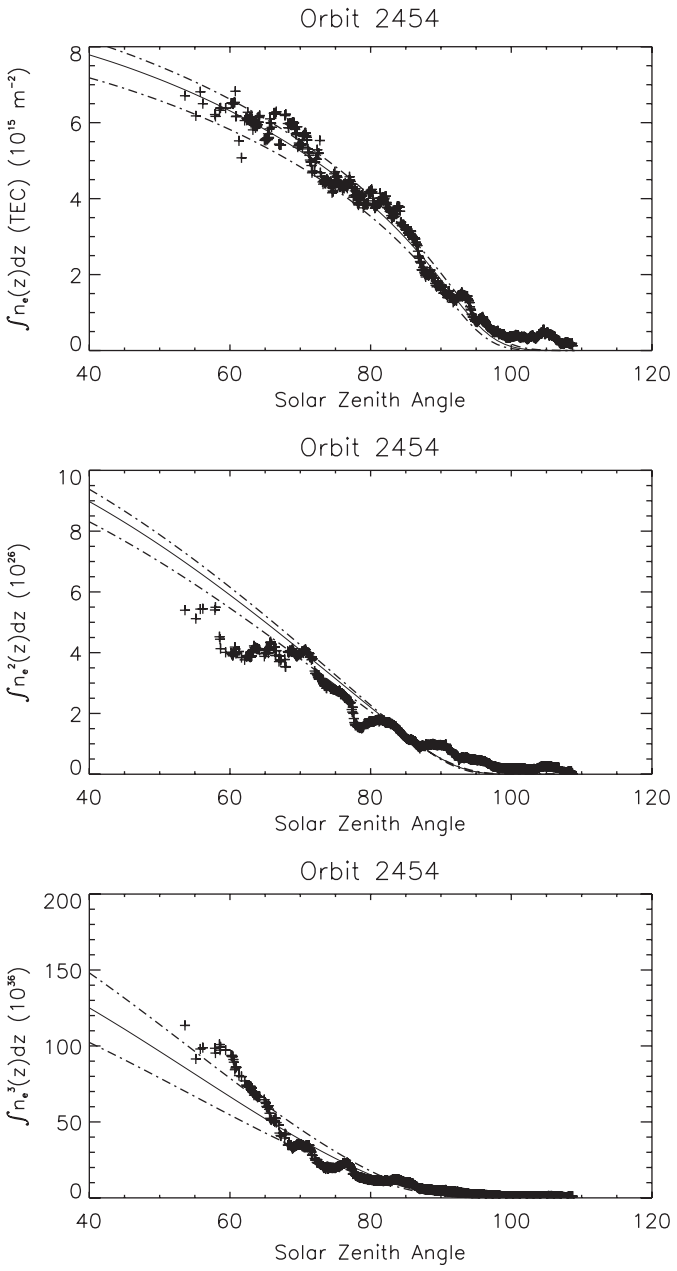

Fig. 6. Fit using α_1, α_2, α_3 as a function of SZA for orbit 2454. We use to fit a Chapman model (Fig. 5) and suppose H and n_0 is constant overall solar zenith angle. Solid line corresponds to the best fit (minimum of ε) and dotted-dashed lines are used to evaluate the sensitivity of the fit parameters n_0 and H.

effect. Therefore a_1, a_2, and a_3 sensitivity is higher for lower bands.

In Fig. 7 we show the TEC variation distribution for the 1 dB variation of the SNR for bands 3 and 4.

A bi-modal behavior appears between day and nighttime. The day and nighttime mean sensitivity on TEC are, respectively, about 3.8×10^{14} and $1.5\times10^{14}\,\mathrm{m}^{-2}$. We can notice that bands 3–4 correspond to highest possible frequencies transmitted in the same time and therefore the associated TEC variation is larger. We show in the Table 1, the estimation of the TEC variability for each couple of frequency. This sensitivity study allows to validate our derived-TEC for future works.

10. Comparison with other TEC result

Many missions, Mariners 4, 6 (Fjeldbo and Eshleman, 1968), Mariner 9 (Kliore et al., 1972), Mars 2, 4, 6 (Vasilev et al., 1975; Kolosov et al., 1976), Viking 1, 2 (Hanson, 1977; Zhang et al., 1990), Mars Global Surveyor MGS (Tyler et al., 2001,), MaRS/MEX (Pätzold et al., 2005) have already recorded electron density profiles which provides us an estimation of TEC (see Mendillo et al., 2003 or Fox and Yeager, 2006 for a more complete summary of these ionospheric measurements). To obtain the TEC, we just integrate overall the density profiles of electron of some of published data.

The Mars Global Surveyor Radio Science experiment provides thousands electron density profiles on a large period and so for different solar activity (Tyler et al., 2001).

In Fig. 8 we show the TEC measured by us compared with measurements obtained during other missions. In this figure measurement from MGS missions (red points) are from the last season (January 1, 2005–June 9, 2005) that are the closer date to data of MARSIS ones (November 2005–January 2006 for Fig. 8) and these two sets of data correspond to periods, where the solar flux is relatively low. The good agreement between MARSIS and MGS data is seen. Mariner 9 occultations have been obtained during moderate solar activity. As expected the TEC values increase with the solar activity and Mariner 9 values of TEC are larger than MARSIS ones. The difference between Mariner 9 and MARSIS is not very pronounced at about 75° but around 50°, Mariner 9 values are higher with TECs close to $10^{16}\,\mathrm{m}^{-2}$ against 0.7×10^{16}–$0.8\times10^{16}\,\mathrm{m}^{-2}$ for MARSIS.

The dependence of TEC values with solar flux is also seen by MARSIS over some period (Safaeinili et al., 2007).

As our data show, MARSIS surface sounding mode is able to derive the TEC values covering a large SZA range in short time (one observation sequence is about 30 min) that have not previously been possible. We estimated only TEC values but have shown that the estimated values can be used to derive useful descriptive parameters for general properties of the Martian ionosphere.

11. Conclusion

MARSIS radar echoes are distorted by the Martian ionosphere. We have developed a robust technique to correct for these distortions and in the correction process obtain information about the ionosphere itself. We can derive information about the ionosphere like the TEC, and electron profiles higher-order moments, $\int n_e^2(h)\,dh$, $\int n_e^3(h)\,dh$ every 2 s. We have shown that these results are in agreement with other data sets. Furthermore, these moments can be used to derive the n_0 and H with

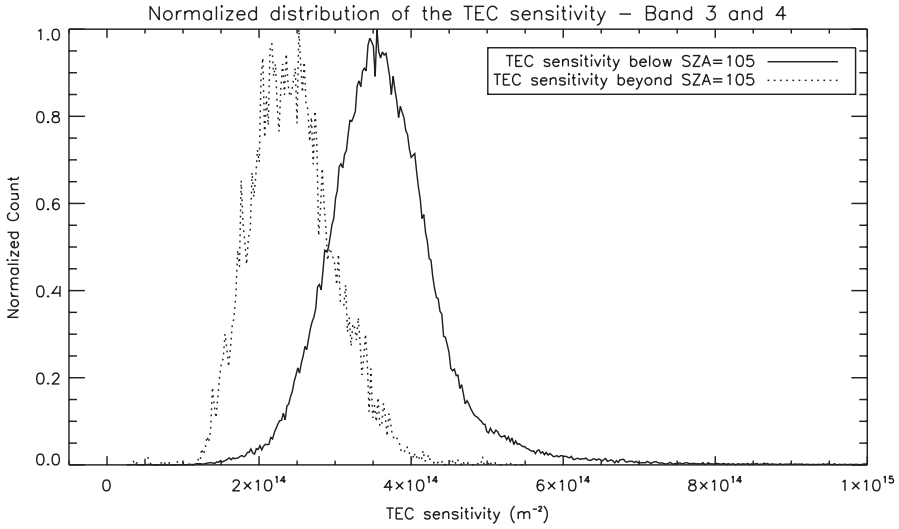

Fig. 7. Normalized distribution of TEC sensitivities for measurements with bands 3 and 4 simultaneously. Dotted line represents sensitivity distribution for solar zenith angle above 105° (complete night) and solid line below 105°.

Table 1
TEC sensitivity that corresponds to a signal power lost of 1 dB compared to the best correction

Combination of MARSIS band	Sensitivity on nighttime TEC (10^{14} m^{-2})	Sensitivity on daytime TEC (10^{14} m^{-2})	Number of measurements for nighttime	Number of measurements for daytime
3–4	2.2	3.5	11,075	138,803
2–4	2	3	440	1830
1–4	1.7	–	1910	0
2–3	1.5	2.6	109,554	54,786
1–3	1.5	2.5	40,066	240
1–2	1	–	10,832	0

These values correspond to the peak of distribution in the Fig. 7. We also give the number of measurements which shows how are combined the different frequency band. Here about 370,000 (only with a significant SNR) pulses were analyzed.

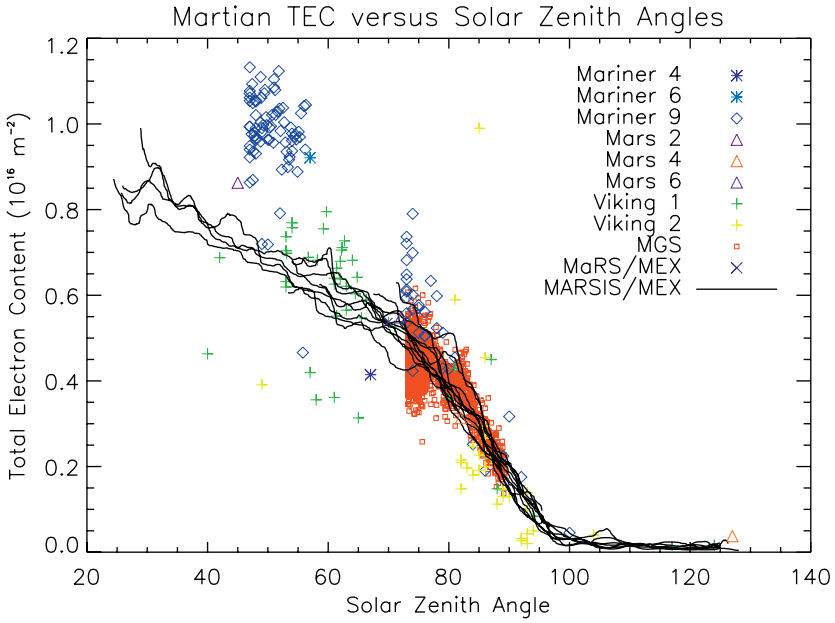

Fig. 8. Total electron content as a function of the solar zenith angle. Each dot corresponds of TEC measurements by other instrument and solid lines to MARSIS TEC measurements in surface sounding mode (see Fig. 4). The altitude ranges can change from a profile to another. For example some profiles may stop at an altitude of 200 km and some other at 300 km. These differences may affect the result on TEC, however, the error due to that is very small because the main electron content (between 100 and 150 km).

typical values has 9.5×10^3 m and 2×10^{11} m^{-3} (Safaeinili et al., 2007).

Due to the large quantity of the TEC estimates from the MARSIS subsurface sounding data we are able to carry out a statistical study of the neutral height scale and peak electron density and also made it possible to map the connection between the nighttime TEC and the magnetic field (in Safaeinili et al., 2007).

Acknowledgments

The authors acknowledge the support of the space agnecies of Italy (ASI) and the United States (NASA), for the development and science operations of MARSIS. Operations of the Mars Express spacecraft by the European Space Agency (ESA) are gratefully acknowledged. The French space agency (CNES) supports these studies in Laboratoire de Planétologie de Grenoble.

References

Banks, P.M., Kockarts, G., 1973. In: Aeronomy. Part A. Academic Press, New York.

Bougher, S.W., Engel, S., Hinson, D.P., Forbes, J.M., 2001. Mars Global Surveyor Radio Science electron density profiles: neutral atmosphere implications. Geophys. Res. Lett. 28, 3091–3094.

Bougher, S.W., Engel, S., Hinson, D.P., Murphy, J.R., 2004. MGS Radio Science electron density profiles: interannual variability and implications for the Martian neutral atmosphere. J. Geophys. Res. (Planets) 109, 3010.

Budden, K.G., 1964. Lectures on Magnetoionoc Theory. Gordon & Breach Publishing Group, London.

Budden, K.G., 1985. The Propagation of Radio Waves. Cambridge University Press, Cambridge.

Chapman, S., 1931. Absorption and dissociative or ionising effects of monochromatic radiation in an atmosphere on a rotating earth. Proc. Phys. Soc., London 43, 1047–1055.

Fjeldbo, G., Eshleman, V.R., 1968. The atmosphere of mars analyzed by integral inversion of the Mariner IV occultation data. Planet. Space Sci. 16, 1035–1059.

Fox, J.L., Yeager, K.E., 2006. Morphology of the near-terminator Martian ionosphere: a comparison of models and data. J. Geophys. Res. (Space Phys.) 111, 10309.

Gurnett, D.A., Kirchner, D.L., Huff, R.L., Morgan, D.D., Persoon, A.M., Averkamp, T.F., Duru, F., Nielsen, E., Safaeinili, A., Plaut, J.J., Picardi, G., 2005. Radar soundings of the ionosphere of Mars. Science 310, 1929–1933.

Hanson, W.B., Sanatani, S., Zuccaro, D.R., 1977. The Martian ionosphere as observed by the viking retarding potential analyzers. J. Geophys. Res. 82, 4351–4363.

Kliore, A.J., Cain, D.L., Fjeldbo, G., Seidel, B.L., Sykes, M.J., Rasool, S.I., 1972. The atmosphere of Mars from Mariner 9 radio occultation measurements (A 5. 5). Icarus 17, 484.

Kolosov, M.A., Ivanov, V.M., Lukin, D.S., Spiridonov, I.G., 1976. Radio occultation of the Martian ionosphere taking into account horizontal gradients of electron density. Space Res., 1013–1017.

Krymskii, A.M., Ness, N.F., Crider, D.H., Breus, T.K., Acuña, M.H., Hinson, D.P., 2004. Solar wind interaction with the ionosphere/atmosphere and crustal magnetic fields at Mars: MARS global surveyor magnetometer/electron reflectometer, radio science, and accelerometer data. J. Geophys. Res. (Space Phys.) 109, 11306.

Mendillo, M., Smith, S., Wroten, J., Rishbeth, H., Hinson, D., 2003. Simultaneous ionospheric variability on Earth and Mars. J. Geophys. Res. (Space Phys.) 108, 1–6.

Nielsen, E., Morgan, D.D., Kirchner, D.L., Plaut, J.J., Picardi, G., 2007. Absorption and reflection of radio waves in the Martian ionosphere. Planet. Space Sci. 55, 864–870.

Picardi, G., Plaut, J.J., Biccari, D., Bombaci, O., Calabrese, D., Cartacci, M., Cicchetti, A., Clifford, S.M., Edenhofer, P., Farrell, W.M., Federico, C., Frigeri, A., Gurnett, D.A., Hagfors, T., Heggy, E., Herique, A., Huff, R.L., Ivanov, A.B., Johnson, W.T.K., Jordan, R.L., Kirchner, D.L., Kofman, W., Leuschen, C.J., Nielsen, E., Orosei, R., Pettinelli, E., Phillips, R.J., Plettemeier, D., Safaeinili, A., Seu, R., Stofan, E.R., Vannaroni, G., Watters, T.R., Zampolini, E., 2005. Radar soundings of the subsurface of Mars. Science 310, 1925–1928.

Pätzold, M., Tellmann, S., Häusler, B., Hinson, D., Schaa, R., Tyler, G.L., 2005. A sporadic third layer in the ionosphere of Mars. Science 310, 837–839.

Safaeinili, A., Kofman, W., Nouvel, J., Herique, A., Jordan, R.L., 2003. Impact of Mars ionosphere on orbital radar sounder operation and data processing. Planet. Space Sci. 51, 505–515.

Safaeinili, A., Kofman, W., Mouginot, J., Gim, Y., Herique, A., Ivanov, A.B., Plaut, J.J., Picardi, G., 2007. Estimation of the total electron content of the Martian ionosphere using radar sounder surface echoes. Geophys. Res. Lett. 34, L23204.

Smith, D., Neumann, G., Arvidson, R. E., Guinness, E. A., Slavney, S., 2003. Mars Global Surveyor Laser Altimeter Mission Experiment Gridded Data Record. NASA Planetary Data System, MGS-M-MOLA-5-MEGDR-L3-V1.0.

Tyler, G.L., Balmino, G., Hinson, D.P., Sjogren, W.L., Smith, D.E., Simpson, R.A., Asmar, S.W., Priest, P., Twicken, J.D., 2001. Radio science observations with Mars global surveyor: Orbit insertion through one Mars year in mapping orbit. J. Geophys. Res. 106, 23327–23348.

Vasilyev, M.B., Vyshlov, A.S., Kolosov, M.A., Savich, N.A., Samovol, V.A., Samoznayev, L.N., Sidorenko, A.I., Aleksandrov, Y.N., Danilenko, A.I., Dubrovin, V.M., 1975. Preliminary results of two-frequency radio-occultation of the Mars ionosphere by means of Mars planetary probes in 1974, NASA STI/Recon Technical Report N, 75, 24625.

Zhang, M.H.G., Luhmann, J.G., Kliore, A.J., 1990. An observational study of the nightside ionospheres of Mars and Venus with radio occultation methods. J. Geophys. Res. 95, 17095–17102.